nature geoscience

LETTERS

PUBLISHED ONLINE: 11 DECEMBER 2011 | DOI: 10.1038/NGEO1342

Anisotropic uppermost mantle in young subducted slab underplating Central Mexico

Teh-Ru Alex Song[1]* and YoungHee Kim[2]

Knowledge of the rate of plate-spreading at mid-ocean ridges is critical for estimating plate motions[1] and the outward flux of heat from Earth's interior[2–4]. Magnetic lineations[5] and anisotropy—crystals that have aligned themselves with mantle flow—preserved in oceanic lithosphere provide a means for estimating plate-spreading rates up to 180 million years ago. However, reconstructions beyond this time are difficult because most older oceanic lithosphere has been subducted into the mantle. Here we use converted seismic waveforms to show that anisotropy is preserved in the subducted part of the Cocos Plate beneath Central Mexico. We observe strong P- and S-wave anisotropy in the topmost 2–6 km of the subducted oceanic mantle. The strength of the anisotropy is comparable to that measured in the surface portion of the Cocos Plate[6]. We also show that P-wave azimuthal anisotropy and plate-spreading rate at present-day mid-ocean ridges exhibit a linear relationship. On the basis of this relationship, we suggest that the subducted portion of the Cocos Plate formed at a half-spreading rate of about 8 cm yr^{-1} at the East Pacific Rise, about 15 million years ago. Our results imply that subducted oceanic lithosphere could preserve an archive of ancient plate-spreading rates on Earth.

Frozen-in seismic anisotropy in the oceanic plates can be demonstrated by observations of azimuthal variations in refracted P-wave (Pn) velocity[7–10], Rayleigh-wave phase velocity[11] and splitting of teleseismic core phases such as SKS waves[11]. In particular, Pn azimuthal anisotropy up to several per cent in the topmost oceanic mantle is strongly linked to a mantle ophiolite section containing anisotropic dunite and harzburgite[12,13]. If such a strong anisotropy can be preserved through subduction and if a relationship between spreading rates and Pn azimuthal anisotropy can be established, it is possible to access palaeo-spreading rates without being limited (to about 180 Myr) by the use of magnetic anomaly lineations.

Recent seismic reflection profiles have shown several shallow-dipping reflectors beneath old continents such as the Slave Craton and the Superior Craton in North America[14–16] that were subsequently characterized as localized mantle anisotropic layers[17–19] and were attributed to several shallow subduction episodes dating back to the Archaean era, supporting subduction stacking as a possible mechanism for the formation of subcratonic lithospheric mantle and stabilization of cratons. If modern analogues of such features can be established, we not only confirm this scenario, but also provide a possible path to infer palaeo-spreading rates. This connection would build an observational ground for reconstruction of plate kinematics and thermal evolution models through the Earth's history[2–4].

We explore the interior of the young subducted Cocos Plate (~15–20 Myr old) now underplating Central Mexico (Fig. 1) because the slab geometry is well defined by recent teleseismic receiver function studies[20] (Supplementary Fig. S1). Furthermore, an ultraslow-velocity layer (USL) in the oceanic crust constrained by local converted S-to-P (SP) waves[21], teleseismic underside reflections[21] and teleseismic receiver functions[20] serves as a reference horizon to search for other possible layering deeper within the slab. We first model another local converted SP wave that consistently arrives about 1–1.2 s after the first P wave to constrain a high-velocity lid (HVL) within the deeper part of the subducted slab below the USL. Subsequently, we simulate teleseismic converted P-to-S waves (equivalently, P-wave receiver functions) to justify that the HVL is a manifestation of an anisotropic layer. The combination of local converted and teleseismic P-wave receiver functions promises a tight constraint on the interior layering and localized anisotropy in the uppermost mantle of the subducted slab (Fig. 1 and Supplementary Information).

We first demonstrate observations and modelling of local SP waves at about 0.03–0.8 Hz in vertical displacement[22]. The direct P wave is typically accompanied by a shoulder bump (Fig. 2a), which is named phase C and is typically 50–70% of the amplitude of the direct P wave. We model phase C as a SP wave converting from a boundary with a negative velocity jump above the earthquake source, which is equivalent to introducing a HVL (Fig. 2a and Supplementary Information). To match the waveforms, we carry out a systematic search on the location, thickness and velocity of the HVL. Our preferred model shows that the lower boundary of the HVL sits about 6–8 km above earthquake sources and exhibits a 7.5±2.5% shear velocity increase with respect to the oceanic mantle directly below the HVL (Fig. 2b). The estimate of lid thickness slightly trades off with lid velocity. As the thickness of the USL is constrained at about 3–5 km (refs 20,21) and the oceanic crust remains 5–7 km thick as it approaches the trench[23], we estimate the thickness of the HVL to be about 2–6 km.

To examine the HVL derived from local converted waves, we investigate teleseismic P-wave receiver functions at the frequency range of 0.03–1 Hz (Fig. 3). In particular, we examine both the radial receiver functions (RRFs) and transverse receiver functions (TRFs), which are sensitive to localized anisotropic layers[24,25]. The receiver functions are primarily constructed using data from events with northwest, southeast and southwest back azimuths recorded by the Middle American Subduction Experiment[20] (MASE). There are strong azimuthal variations in the amplitude and/or polarity of converted P-to-S waves in the RRFs as well as TRFs (Fig. 3). Our preferred model parameters are principally constrained by RRFs and the local converted arrivals. The TRFs are noisier and we mostly refer to Fig. 3 and Supplementary Fig. S2 to examine general consistency between data and synthetics.

[1]Interior for Research on Earth Evolution (IFREE), Japan Agency for Marine-Earth Science and Technology Center (JAMSTEC), 3173-25 Showa-machi, Kanazawa-ku, Yokohama City, Kanagawa 237-0005, Japan, [2]Division of Geological and Planetary Science, California Institute of Technology, 1200 E. California Blvd, Pasadena, California 91125, USA. *e-mail: tehrusong@gmail.com.

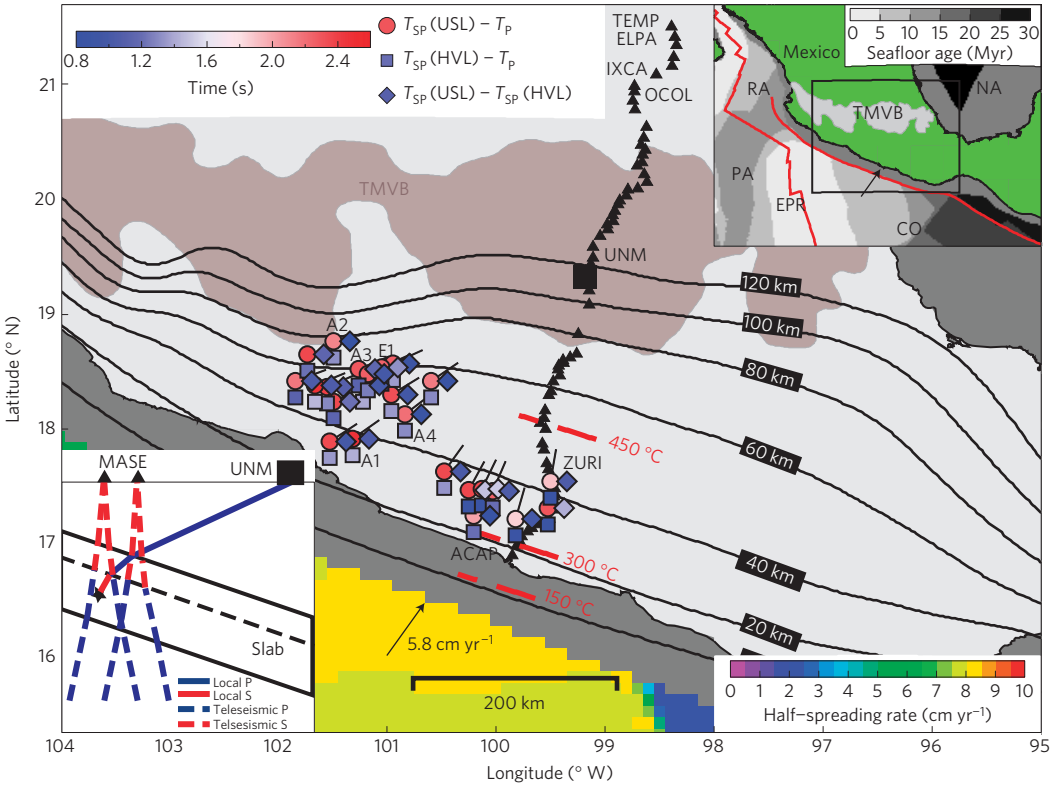

Figure 1 | Seismic probe of the subducted Cocos Plate beneath the Central Mexico subduction zone. Tectonic framework with slab isodepth contours[29] (solid black lines), plate motion direction (solid arrow) and slab surface temperature[30] (red dashed lines). Differential times among the first P wave, converted SP waves from the USL and converted SP waves from the HVL recorded at station UNM are shown by coloured symbols. Spreading rates and plate ages estimated from magnetic anomaly lineations[5] are shown in the main diagram and upper inset, respectively. Triangles mark the stations of the MASE. The lower-left inset illustrates the ray geometry. RA, Rivera Plate; NA, North America Plate; CO, Cocos Plate; PA, Pacific Plate; TMVB, Trans-Mexican Volcanic Belt; EPR, East-Pacific Rise. Local waveforms from events A1–4 and E1 recorded by the UNM station and MASE stations OCOL, IXCA, ELPA and TEMP are shown in Fig. 2. Stations ACAP and ZURI mark the end of the receiver function profile shown in Fig. 3.

In the RRFs, we observe a strong negative pulse converted from the top of the USL followed by a moderate positive pulse contributed from the bottom of the USL and the top of the HVL in the southeast swath (Fig. 3a). A strong and positive pulse contributed from the bottom of the USL and the top of the HVL is observed in the northwest swath with weak negative pulses arriving just before and after this strong positive pulse. The positive arrival also exhibits a broader pulse width in the southeast swath than those observed in the northwest swath. In the southwest swath, the amplitude of RRFs is relatively small with complicated and mixed polarities (Fig. 3a).

Although the effect of slab dip can change the amplitude of all converted arrivals in the RRFs in a consistent manner[26], observed azimuthal variations in the relative amplitude among converted arrivals indicate that the USL and HVL may both be strongly anisotropic. These observational features can be consistently recognized when different stacking procedures are implemented (Supplementary Fig. S2). We focus on the HVL detected by modelling local converted SP waveforms and conclude that it can be reconciled with an anisotropic layer from modelling teleseismic receiver functions (see Methods).

Our modelling result indicates that the azimuth and dip of the fast symmetry axis of the anisotropic layer are constrained with uncertainties of about ±10° and the azimuth is generally consistent with the direction of subduction (~35° N, Fig. 1). We note that a tilted fast symmetric axis in the model makes it possible to constrain the P-wave anisotropy[24] with receiver functions, but difficult to constrain the S-wave anisotropy with receiver functions alone. Therefore, we project the S-wave anisotropy in the receiver function to the direction of the local SP wave, which yields an estimated anisotropy of about 7%, which is comparable to the S velocity contrast obtained from modelling the local SP wave (~7.5%, Fig. 2c).

The anisotropic layer is observed in the depth ranges of 28–53 km and it is about 6–12 km below the slab surface. Considering the pressure and temperature condition appropriate at this depth, the lithology of the anisotropic layer is probably depleted harzurgites as well as dunites, which can be found in the mantle section of ophiolite outcrops (Supplementary Information). They have been strained by asthenosphere flows to form strong fabric alignment[12,13,27] and are the source of observed Pn azimuthal anisotropy.

We compile recent Pn azimuthal anisotropy obtained from modern multi-channel seismics at northern East Pacific Rise[7], Mid-Atlantic Ridge[8] and northwestern Pacific Plate localities[9,10] where plate age and half-spreading rate vary. Although the strength of seismic anisotropy and the orientation of the fast symmetric axis probably do depend on many variables such as strain rate, temperature, volatile and melt fraction[27] and reflect the balance between passive flow and active upwelling (Supplementary Information), these observations form a linear relationship between the half-spreading rate and Pn azimuthal anisotropy (Fig. 4 and Supplementary Fig. S14).

As the Pn azimuthal anisotropy is a measure of velocity anisotropy on the horizontal plane, we project the anisotropy of the anisotropic layer to the horizontal plane and find that it falls close to this linear relationship (Fig. 4 and Supplementary Fig. S14). This indicates that the anisotropy in the anisotropic layer initially formed in the East Pacific Rise is probably not overprinted by later processes such as deformation in the outer rise and subsequent underplating beneath Central Mexico. Recent geodynamic models also support

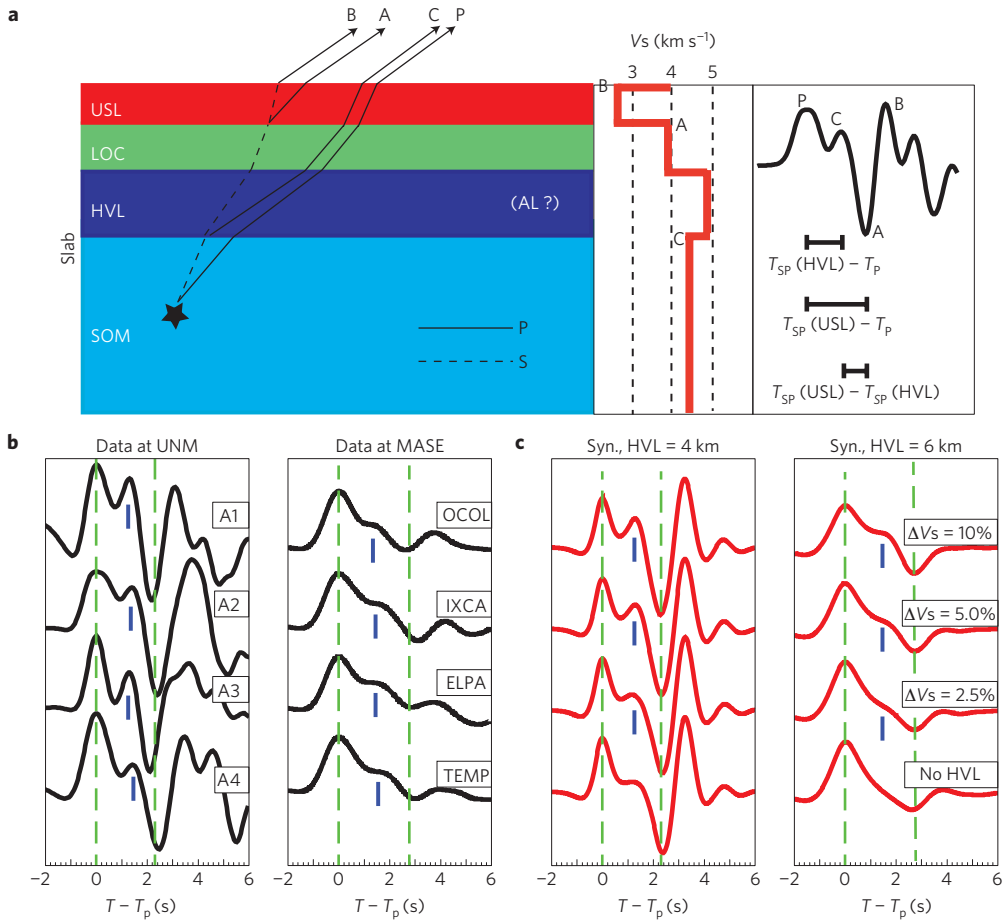

Figure 2 | Observations and finite-difference modelling of local converted SP waves. a, Diagram showing the ray paths of direct P wave (P) and converted SP waves (A, B and C), the shear velocity (*Vs*) profile within the slab and a typical P waveform. LOC, lower oceanic crust; SOM, subducted oceanic mantle. **b**, Observations of local SP waveforms from events A1, A2, A3 and A4 at the UNM station and from event E1 at the MASE stations. SP waves from the USL are marked by green dashed lines. **c**, Synthetics calculated with different velocity contrast in the HVL and without the USL (right panel) against waveform data in **b**. Blue bars depict the observed and calculated SP waves from the HVL. d*Vs*, perturbation of S-wave velocity. The HVL is demonstrated later by receiver function analysis as a manifestation of an anisotropic layer (AL).

the presence of a low-viscosity channel[28], which may help decouple the slab from the overriding plate and preserve the anisotropic layer.

Here we conclude that the anisotropic layer in the subducted Cocos Plate and Pn azimuthal anisotropy observed on the sea floor are probably of common origin and they represent the frozen-in anisotropy in the topmost oceanic mantle. Such a strong anisotropy localized within the top few kilometres of the subducted mantle is also consistent with the strong fabric development generally observed in the topmost mantle section of ophiolites[13], which is composed of strained dunite and depleted harzburgite assemblages. In addition, the fast symmetric axis of the anisotropic layer is dipping towards the subduction direction and away from the East Pacific Rise, which could be indicative of processes relevant to anisotropy generation processes near the mid-ocean ridges (MORs; Supplementary Information).

Together, the anisotropic layer constrained by local converted waves and receiver function analysis is more precisely described as an anisotropic mantle lid (AML) within the subducted Cocos Plate. Our finding may have particularly important implications for interpretation of the dipping anisotropic layers found beneath cratons[17–19]. Along with continuous dipping reflection images from active-source seismic surveys that are collocated with these anisotropic layers[15–18], these dipping anisotropic layers beneath the Wopmay Orogen[18], the western Slave Craton[17] and the Superior Craton[19] in Canada have been linked to shallow subduction episodes in the late Archaean to early Proterozoic eras and are signatures of relic slabs preserved over billions of years.

In particular, the dipping anisotropic layer beneath the Wopmay Orogen has a fast symmetry axis dipping towards the subduction direction, but it is dipping more steeply, at about 70° from the horizontal axis. The P-wave and S-wave anisotropy are about 5%, almost 50% less than estimates in the AML within the subducted Cocos Plate. On the other hand, the anisotropic layer beneath the western Slave Craton is suggested to have a rather shallow-dipping fast symmetric axis with 5.5% anisotropy, similar to the anisotropic layer beneath the Superior Craton.

A recent study suggests that these dipping anisotropic layers beneath the Wopmay Orogen and the western Slave Craton are depleted mantle layers that were either formed *in situ* beneath the craton or were synthesized at ancient MORs and later subducted[17,18]. Our finding that the AML in the Cocos Plate survives subduction and is visible beneath Central Mexico indicates that the AML is very likely a modern analogue of those dipping anisotropic layers found beneath cratons (Supplementary Fig. S15) and strongly favours the latter scenario for formation of the Archaean dipping layers.

If palaeo-AMLs beneath cratons were indeed formed at palaeo-MORs and later subducted beneath cratons, we may be able to infer the half-spreading rates of these long-vanished ridges with the linear relationship established previously, assuming it is

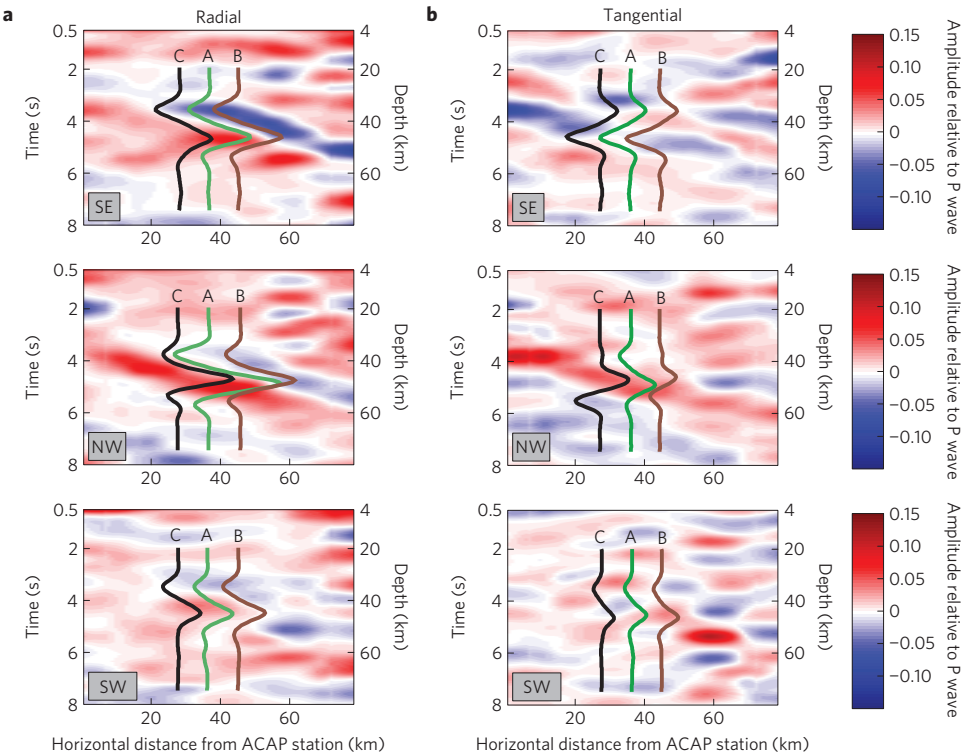

Figure 3 | Stacked receiver function images and modelling. a, RRF images produced by assigning the amplitude of stacked RRFs within a spatial grid and linear interpolation among stations constructed for different back azimuths, colour-coded according to the absolute amplitude. The detail processing is the same as in ref. 20. Synthetics computed from an isotropic dipping USL (model A, green traces), an anisotropic dipping USL (model B, brown traces) and an anisotropic dipping USL and an anisotropic layer (model C, black traces) are shown against azimuth-dependent receiver functions. **b**, The same as in **a**, but for stacked P-wave TRF images and synthetics.

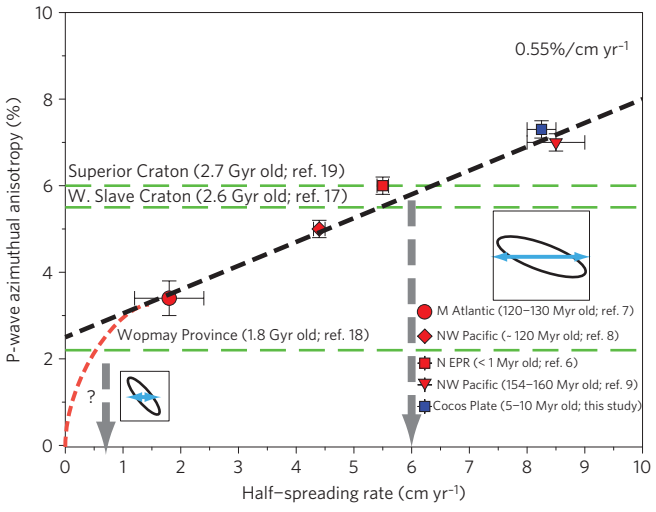

Figure 4 | P-wave azimuthal anisotropy versus half-spreading rates. The observation (blue square) defined by azimuthal anisotropy projected from the AML and a half-spreading rate from pre-subducted Cocos Plate (~8 cm yr^{-1}, see also Fig. 1) is in agreement with the established relationship between observed Pn azimuthal anisotropy[7–10] (red symbols) and half-spreading rates (black dashed line, a slope of ~ 0.55 %/cm yr^{-1}). The azimuthal anisotropy projected from palaeo-AML (refs 17–19; green dashed lines) is used to infer the palaeo-half-spreading rates (dashed arrows). The hexagonal anisotropy in the AML and palaeo-AML (ref. 18) are schematically shown as ellipses, with their sizes proportional to the strength of the anisotropy, and horizontal double arrows corresponding approximately to the strength of the anisotropy projected on the horizontal plane.

time invariant (Fig. 4). Future analysis of AMLs within subducted oceanic mantle and continental lithosphere around the world and increasing sampling of Pn azimuthal anisotropy on ocean sea floor will help shed new light on plate kinematics in early Earth but also clarify the role of slab underplating in craton stabilization and subcratonic lithosphere formation.

Methods

Here we describe details of the modelling of RRFs in the main text and the process leads to the conclusion of the anisotropic layer in the subducted Cocos Plate. Starting with a background model that is derived from modelling local converted waveforms, we compute synthetic receiver functions[25] for an isotropic dipping USL and HVL (Supplementary Fig. S3 and Table S1). We find that synthetic converted P-to-S waves are consistently strong in the northwest swath and weak in the southeast swath (model A, Fig. 3a). The negative arrival associated with the top of the USL is predicted to be strong in the southeast swath and weak in the northwest swath, which are entirely opposite to our observations. Such a strong azimuthal variation in the amplitude of converted arrivals associated with the USL probably indicates a shallow-dipping fast symmetric axis.

Assuming a hexagonal anisotropy model, we carry out a grid search to look for the azimuth (φ) and dip (δ) of the fast symmetric axis in the USL (Supplementary Fig. S4a,b). Synthetics including a strong anisotropic USL (P-wave anisotropy, 10%, S-wave anisotropy, 10%; $\varphi = 0°$ N, $\delta = 30°$) can reproduce the relative strength of the negative converted arrival from the top of the USL in different back azimuths (model B, Fig. 3a and Supplementary Figs S5–S7) as well as their absolute amplitude.

However, an anisotropic USL alone does not explain the strong positive arrival observed solely in the northwest swath and a broader pulse observed in the southeast swath. Therefore, we also carry out a grid search to look for the azimuth (φ) and dip (δ) of the fast symmetric axis in the HVL (Supplementary Fig. S4a,c). As the HVL is derived from isotropic modelling of local converted arrivals, it is likely that an anisotropic layer is manifested as an isotropic HVL, especially when the fast symmetric axis is subhorizontal and at a large angle to the incident local S wave. Thereafter, we replace the HVL with an anisotropic layer so that the isotropic velocity in the anisotropic layer is no different from the medium below it.

Synthetics that include a strong anisotropic layer (P-wave anisotropy, 10%, S-wave anisotropy, 10%; $\varphi = 30°$ N, $\delta = 40°$) are capable of reproducing the

strong positive arrival in the northwest swath and a broader pulse width in the southeast swath (model C, Fig. 3a and Supplementary Figs S8–S10). The strong positive arrival observed in the northwest swath is apparently due to constructive interferences between energy from the bottom of the USL and the top of the anisotropic layer in this azimuth. Finally, the weak converted arrivals observed in the southwest swath are also predicted reasonably well, but the sensitivity of these arrivals to anisotropic model parameters is relatively low.

We examine a few key observations in the TRFs against our model (Fig. 3b). The converted arrivals in the TRFs seem variable and weaker than predictions from the dipping slab in a few recordings (model A, Fig. 3b and Supplementary Fig. S11). We note that a steeper fast symmetric axis of the USL ($\delta = 40°$–$50°$) can be consistent with weak signals in some stations in the southeast-swath TRFs (Supplementary Fig. S6). In general, the amplitude of TRFs seems smaller than that of RRFs, and they have opposite polarity in the southeast swath. However, in the northwest swath, we observe an extremely subtle arrival from the top of the USL. In addition, strong positive and negative arrivals from the bottom of the USL and the top of the anisotropic layer are almost equal in amplitude, which is explained only by anisotropy in both the USL and the anisotropic layer.

All of these observations provide constraints on the strength of anisotropy and the orientation of the fast symmetric axis in the USL and the anisotropic layer (models B and C, Fig. 3b and Supplementary Figs S5–S10). We emphasize that the anisotropic model is principally constrained by the local converted arrivals as well as RRFs. TRFs are generally noisier and we examine gross consistency between observed and synthetic TRFs. These preferred model parameters also explain RRFs and TRFs observed directly above the flat section of the subducted Cocos Plate (Supplementary Fig. S12) reasonably well, including double positive arrivals occasionally observed in the RRFs in the southeast swath (Supplementary Fig. S13).

Received 24 March 2011; accepted 10 November 2011; published online 11 December 2011

References

1. DeMets, C., Gordon, R. G. & Argus, D. F. Geologically current plate motions. *Geophys. J. Int.* **181,** 1–80 (2010).
2. Becker, T. W., Conrad, C. P., Buffet, B. & Muller, R. D. Past and present seafloor age distribution and temporal evolution of plate tectonic heat transport. *Earth Planet. Sci. Lett.* **278,** 233–242 (2009).
3. Labrosse, S. & Jaupart, C. Thermal evolution of the Earth: Secular changes and fluctuations of plate characteristics. *Earth Planet. Sci. Lett.* **260,** 465–481 (2007).
4. Korenaga, J. *Archean Geodynamics and Environments* Vol. 164, 7–32 (AGU Monograph Series, AGU, 2006).
5. Muller, R. D., Sdrolias, M., Gaina, C. & Roest, W. R. Age, spreading rates and spreading symmetry of the world's ocean crust. *Geochem. Geophys. Geosys.* **9,** Q04006 (2008).
6. Sndysman, W. E., Lewis, B. T. R. & McClain, J. Upper mantle velocities on the northern Cocos plate. *Earth Planet. Sci. Lett.* **28,** 46–50 (1975).
7. Toomey, D. R., Jousselin, D., Dunn, R. A., Wilcock, W. S. D. & Detrick, R. S. Skew of mantle upwelling beneath the East Pacific Rise governs segmentation. *Nature* **446,** 409–414 (2007).
8. Gaherty, J. B., Lizarralde, D. L., Collins, J., Hirth, G. & Kim, S. Mantle deformation during slow seafloor spreading constrained by observations of seismic anisotropy in the western Atlantic. *Earth Planet. Sci. Lett.* **228,** 255–265 (2004).
9. Shinohara, M. *et al.* Upper mantle and crustal seismic structure beneath the northwestern Pacific basin using a seafloor broadband seismometer and ocean bottom seismometers. *Phys. Earth Planet. Inter.* **170,** 95–106 (2008).
10. Oikawa, M., Kaneda, K. & Nishizawa, A. Seismic structures of the 154–160 Ma oceanic crust and uppermost mantle in the northwest Pacific Basin. *Earth Planets Space* **62,** E13–E16 (2010).
11. Park, J. & Levin, V. Seismic anisotropy: Tracing plate dynamics in the mantle. *Science* **296,** 485–489 (2002).
12. Christensen, N. I. The magnitude, symmetry and origin of upper mantle anisotropy based on fabric analyses of ultramafic tectonites. *Geophys. J. R. Astr. Soc.* **76,** 89–111 (1984).
13. Ismail, W. B. & Mainprice, D. An olivine fabric database: an overview of upper mantle fabrics and seismic anisotropy. *Tectonophysics* **296,** 145–197 (1998).
14. Calvert, A. J., Sawyer, E. W., Davis, W. J. & Ludden, J. N. Archaean subduction inferred from seismic images of a mantle suture in the Superior Province. *Nature* **375,** 670–674 (1995).
15. Cook, F., van der Velden, A. J., Hall, K. W. & Roberts, B. J. Frozen subduction in Canada's northwest territories: Lithoprobe deep lithospheric reflection profiling of the western Canadian shield. *Tectonics* **18,** 1–24 (1999).
16. Van der Velden, A. J. & Cook, F. Relict subduction zones in Canada. *J. Geophys. Res.* **110,** B08403 (2005).
17. Bostock, M. G. Anisotropic upper-mantle stratigraphy and architecture of the Slave craton. *Nature* **390,** 392–395 (1997).
18. Mercier, J-P. *et al.* The teleseismic signature of fossil subduction: Northwestern Canada. *J. Geophys. Res.* **113,** B04308 (2008).
19. Masacchio, G., White, D. J., Asudeh, I. & Thomson, C. J. Lithospheric structure and composition of the Archaean western Superior Province from seismic refraction/wide-angle reflection and gravity modelling. *J. Geophys. Res.* **109,** B03304 (2004).
20. Kim, Y., Clayton, R. W. & Jackson, J. M. Geometry and seismic properties of the subducting Cocos plate in central Mexico. *J. Geophys. Res.* **115,** B06310 (2010).
21. Song, T-R. A. *et al.* Subducting slab ultra-slow velocity layer coincident with silent earthquake in southern Mexico. *Science* **324,** 502–506 (2009).
22. Helmberger, D. V. & Vidale, J. Modeling strong motions produced by earthquakes with two-dimensional numerical codes. *Bull. Seismol. Soc. Am.* **78,** 109–121 (1988).
23. Shor, G. G. & Fisher, R. L. Middle America trench: Seismic refraction studies. *Geol. Soc. Am. Bull.* **72,** 721–729 (1961).
24. Levin, V. & Park, J. P-SH conversions in layered media with hexagonally symmetric anisotropy: A cookbook. *Pure Apply. Geophys.* **151,** 669–697 (1998).
25. Frederiksen, A. W. & Bostock, M. G. Modeling teleseismic waves in dipping anisotropic structures. *Geophys. J. Int.* **141,** 401–402 (2000).
26. Cassidy, J. F. Numerical experiments in broadband receiver function analysis. *Bull. Seismol. Soc. Am.* **82,** 1453–1474 (1992).
27. Karato, S., Jung, H., Katayama, I. & Skemer, P. Geodynamic signatures of seismic anisotropy of the upper mantle: New insights from laboratory studies. *Annu. Rev. Earth Planet. Sci.* **36,** 59–95 (2008).
28. Manea, V. & Gurnis, G. Subduction zone evolution and low viscosity wedges and channels. *Earth Planet. Sci. Lett.* **264,** 22–45 (2007).
29. Pardo, M. & Suarez, G. Shape of the subducted Rivera and Cocos plates in southern Mexico, seismic and tectonic implications. *J. Geophys. Res.* **100,** 12357–12373 (1995).
30. Currie, C. A., Hyndman, R. D. & Wang, K. Thermal models of the Mexico subduction zone: Implications for the megathrust seismogenic zone. *J. Geophys. Res.* **107,** 2370 (2002).

Acknowledgements

We are grateful to the Incorporated Research Institutions for Seismology Data Management Center (IRIS-DMC) for making the data available. We thank A. Federiksen and M. Bostock for providing software for calculating receiver functions through dipping anisotropic layers, and H. Kawakatsu, P. Asimow and S. O'Reilly for the comments on lithospheric anisotropy, ophiolite assemblages and cratonic lithosphere formation during the early stage of this work. We acknowledge the MASE team for making the data available. We also thank D. Anderson and P. D. Asimow for help in reviewing an early draft of this paper. This study is supported by the Institute for Research on Earth Evolution (IFREE), Japan Agency for Marine-Earth Science and Technology (JAMSTEC) and the Tectonic Observatory at Caltech.

Author contributions

T-R.A.S. initiated the project and carried out local waveform modelling. T-R.A.S. and Y.K. carried out receiver function analysis and modelling. T-R.A.S. and Y.K. wrote the manuscript.

Additional information

The authors declare no competing financial interests. Supplementary information accompanies this paper on www.nature.com/naturegeoscience. Reprints and permissions information is available online at http://www.nature.com/reprints. Correspondence and requests for materials should be addressed to T-R.A.S.